Generation of hard X-rays using an ultrafast fiber laser system

Kai-Hsiu Liao, Aghapi G. Mordovanakis, Bixue Hou, Guoqing Chang, Matthew Rever, Gerard Mourou, John Nees, and Almantas Galvanauskas

Center for Ultrafast Optical Science, University of Michigan
2200 Bonisteel Blvd., Ann Arbor, MI, USA 48109
liaok@umich.edu

Abstract: We report the first hard X-ray source driven by a femtosecond fiber laser. The high energy fiber CPA system incorporated a 65μm LMA fiber amplifying stage which provided 300-fs recompressed pulses and diffraction limited beam quality with $M^2 < 1.07$. A deformable mirror was used to optimize the wavefront and the spot size was focused down to 2.3 μm with an *f*/1.2 paraboloidal mirror. 50μJ was deposited on the nickel target with $2x10^{15}$-W/cm^2 focal intensity and a distinctive Ni K_α-line (7.48 keV) emission was measured with $5x10^{-8}$ energy conversion efficiency.

OCIS codes: (140.3510) Laser, fiber; (140.7090) Ultrafast lasers; (140.7240) UV, XUV, X-ray lasers.

References and links

1. C. W. Siders, A. Cavalleri, K. Sokolowski-Tinten, Cs. T´oth, T. Guo, M. Kammler, M. Horn von Hoegen, K. R. Wilson, D. von der Linde and C. P. J. Barty, "Detection of nonthermal melting by ultrafast x-ray diffraction," Science **286,** 1340–1342 (1999).
2. C. Rischel, A. Rousse, I. Uschmann, P. A. Albouy, J. P. Geindre, P. Audebert, J. C. Gauthier, E. Forster, J. L. Martin, and A. Antonetti, "Femtosecond time-resolved X-ray diffraction from laser-heated organic films," Nature (London) **390,** 490–492 (1997)
3. R. Toth, J. C. Kieffer, S. Fourmaux, T. Ozaki, and A. Krol, "In-line phase-contrast imaging with a laser-based hard x-ray source," Rev. Sci. Instrum., **76**, 083701–0837067 (2005).
4. E. Andersson, G. Hölzer, E. Forster, M. Gratz, L. Kiernan, A. Sjogren, S. Svanberg, "Coronary angiography using laser plasma sources: X-ray source efficiency and optimization of a bent crystal monochromator," J. Appl. Phys. **90,** 3048–3056 (2001).
5. A. Mordovanakis, K.-C. Hou, Y.-C. Chang, M.-Y. Cheng, J. Nees, B. Hou, A. Maksimchuk, G. Mourou and A. Galvanauskas, "Demonstration of fiber-laser-produced plasma source and application to efficient extreme UV light generation," Opt. Lett. **31,** 2517–2519 (2006).
6. K. -H. Liao, K. -C. Hou, G. Chang, V. Smirnov, L. Glebov, R. Changkakoti, P. Mamidipudi, and A. Galvanauskas, "Diffraction-Limited 65-μm Core Yb-Doped LMA Fiber Based High Energy Fiber CPA Systems," in *Conference on Lasers and Electro-Optics/Quantum Electronics and Laser Science Conference and Photonic Applications Systems Technologies*, Technical Digest (CD) (Optical Society of America, 2006), paper CPDB4.
7. M. Hagedorn, J. Kutzner, G. Tsilimis and H. Zacharias "High-repetition-rate hard x-ray generation with submillijoule femtosecond laser pulses,"Appl. Phys. B, **77,** 49–57, (2003).
8. B. Hou, J. Nees, A. Mordovanakis, M. Wilcox, G. Mourou, L.M. Chen, J.-C. Kieffer, C.C. Chamberlain and A. Krol "Hard x-ray generation from solids driven by relativistic intensity in the lambda-cubed regime," Appl. Phys. B, **83,** 81–85 (2006).
9. K. -H. Liao, M. -Y. Cheng, E. Flecher, V. I. Smirnov, L. B. Glebov, and A. Galvanauskas, "Large-aperture chirped volume Bragg grating based fiber CPA system," Opt. Express **15**, 4876-4882 (2007)

1. Introduction

Ultrafast X-ray sources are instrumental in the atomic and molecular structural dynamics studies with atomic-scale spatial and sub-picosecond temporal resolutions. Up to date synchrotron-based sources have been prevalently used in such studies due to their high brightness. However, obvious practical limitations associated with the use of synchrotron sources lead to the necessity to search for more practical alternatives. In general, laser produced X-ray sources provide with a more practical approach suitable for a variety of

#86447 - $15.00 USD Received 13 Aug 2007; revised 13 Sep 2007; accepted 22 Sep 2007; published 9 Oct 2007

applications ranging from solid state physics [1] to the biological sciences [2], such as phase contrast imaging [3] and coronary angiography [4]. In addition, due to the small diameter of a laser produced plasma source it can achieve imaging resolution impractical with conventional X-ray tubes. This makes such plasma X-ray sources interesting to medical and industrial radiography.

Until recently, the generation of laser driven ultrafast X-ray radiation were mainly performed with high energy solid-state laser technology which is reaching maturity and lacks sufficient average output power to generate enough X-ray photon flux for a number of practical applications. In recent years, technological advances in the development of mega-watt peak-power, high average-power pulsed fiber lasers have made them an attractive source for the generation of short wavelength radiation [5]. Fiber chirped pulse amplification (FCPA) system are also rapidly developing and have reached the millijoule range [6]. This achievement opens the possibility of practical high-brightness table-top laser driven hard X-ray source using a high energy and high average power fiber laser system as the driver. In this paper, we report the first demonstration of a high energy fiber laser driven K_α-line emission using a solid nickel (Ni) target (7.48 keV) with 300-fs pulses. The energy conversion efficiency was $5x10^{-8}$ which is comparable with previous result using Ti:sapphire laser with similar pulse energies.

2. Ultrafast fiber laser driver

In order to achieve hard X-ray generation using an ultrafast fiber laser system, it was necessary to generate a sufficiently hot plasma by using as high an intensity as possible on the target while keeping the temporal pulse profile as clean as possible to prevent the generation of detrimental plasma expansion before the arrival of the main pulse. Thus, in order to achieve hard X-ray generation using an ultrafast fiber laser, it needs to provide not only close to the state-of-the-art sub-picosecond high-energy pulses but must do so with sufficiently high pre-pulse contrast.

An FCPA system was constructed at 1μm wavelength utilizing high-efficiency ytterbium (Yb) doped fiber amplifiers. A long stretched pulse duration stretcher and a very-large-mode-area (VLMA) fiber amplifying stage were incorporated into the system in order to facilitate energy extraction with minimal nonlinear effects, mainly self-phase modulation (SPM). The schematic of the FCPA driver for hard X-ray generation is shown in Fig. 1. It consists of an ultrafast solid-state mode-locked oscillator (femtoTRAIN, High Q laser), a diffraction grating based stretcher, four amplifying stages, and a diffraction grating based compressor.

The seed pulses of the FCPA system were transform limited 100-fs, 1.8-nJ pulses at 72-MHz repetition rate. The center wavelength was 1064 nm with 11-nm FWHM bandwidth. Pulses from the oscillator were launched directly into a diffraction grating based stretcher. A high-dispersive 1800-line/mm gold surface grating was used to stretch the pulse to ~1-ns. It should be noted that the both temporal and spectral profiles are of the same shape for strongly chirped pulses. When the long stretched pulses were tailored to fast rising and falling edges in the temporal domain in order to maximize energy extraction, it also possesses sharp rising and falling edges in the spectral domain. Therefore, the stretcher was not designed to preserve the entire bandwidth of the signal from the oscillator but only to accommodate 10-nm bandwidth centered at 1064 nm to facilitate energy extraction from the FCPA system. Firstly, spectral clipping eliminates the spectral tails and provides a stretched pulse which has a closer resemblance to a square temporal profile. Thus, the extracted energy can be higher while having the same stretched pulse peak power. Secondly, a narrower spectral width alleviates gain narrowing and frequency pulling effects due to the tilted gain profile at 1064 nm in the Yb amplifying chain so that narrowing of the stretched pulse is reduced and energy extraction is increased. A Pockels cell with 13-ns window and 50dB extinction ratio was placed after the stretcher to down convert pulse repetition rate to 1 kHz.

The repetition-rate-down-converted pulses were then coupled back into a four-stage fiber amplifying chain consisting of two single-mode (SM) fiber preamplifiers, a 30-μm-core large-mode-area (LMA) fiber amplifier, and finally a 65-μm-core VLMA fiber amplifier. Both of

#86447 - $15.00 USD Received 13 Aug 2007; revised 13 Sep 2007; accepted 22 Sep 2007; published 9 Oct 2007

the SM preamplifiers use 3-m single-clad core-pumped highly-doped Yb fibers which were pumped at 974 nm. The first preamplifier was in a counter-propagating pumping scheme to increase the gain while the second preamplifier was in a co-propagating pumping configuration in order to prevent energy damage to the wavelength-division-multiplexer (WDM) and eliminate unnecessary passive fiber after the gain fiber. This would shorten the effective propagation length in the single-mode fiber and thus minimize undesirable nonlinear effects. The two preamplifiers are separated by an inline isolator and an acousto-optic modulator (AOM), with a 70-ns rise time, to prevent feedback and crosstalk. The pulse energy reached 500 nJ after the second preamplifier.

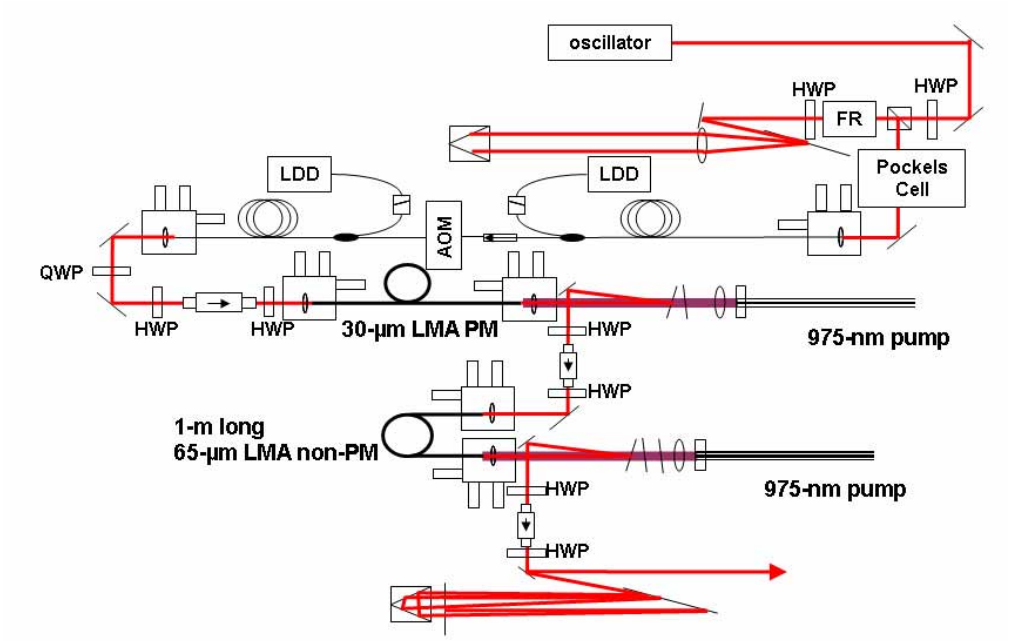

Fig. 1. Schematic of the high energy FCPA system for X-ray generation. It uses a solid-state oscillator as a seeder. Pulse stretching and recompression are done by conventional metal-surface diffraction grating based stretcher and compressor. Four amplifiers, two single-mode, one 30-µm-core LMA amplifier and one 65-µm-core VLMA amplifiers, are used in the amplifying chain.

The signal from the preamplifier was injected into a 3-m long, 30/250 (µm-core/µm-clad) Yb-doped polarization maintaining (PM) with numerical apertures of 0.062 and 0.47 for core and cladding, respectively. Since different modes propagate at a different group velocity in the multimode fiber and thus will result in a pulse train after pulse recompression, single-mode operation is required for multimode fiber used in FCPA systems. The fundamental mode operation was achieved by coiling the 3-m long 30-µm-core LMA fiber on an 8-cm-diameter disk to filter out unwanted high order modes. To both ends of the 30-µm-core fiber, a 4-mm long coreless protective end-cap in order to prevent surface damage at high energies and angle polished at 12° to eliminate feedback from the Fresnel reflection. As can be seen in Fig. 1, this stage was counter-propagating pumped at 975 nm with a free-space coupling arrangement. The pulse energy reached 11 µJ at the output end of the 30-µm-core stage.

The last stage of this multiple stage amplifier chain was a non-PM 65/400 (µm-core/µm-clad) VLMA fiber with numerical apertures of 0.062 and 0.47 for the core and cladding, respectively. Calculated and measured mode-field-diameter (MFD) is 50-µm. Single-mode excitation technique was used for the 65-µm-core fiber to achieve a diffraction-limited beam at the output of the fiber CPA system. Care has to be taken to ensure that both ends of the

#86447 - $15.00 USD Received 13 Aug 2007; revised 13 Sep 2007; accepted 22 Sep 2007; published 9 Oct 2007

fiber were mounted with minimal amount of mechanical stress and there was no unnecessary fiber bending and twisting. With precise matching of the MFD between the 30-μm-core and 65-μm-core fibers (using carefully selected lenses), single-mode operation of the 65-μm-core fiber was achieved with $M^2 < 1.07$ which was consistent with the observed SM profile for both near and far fields. The M^2 measurement and coupled-charge device (CCD) camera measured beam profile are shown in Fig. 2. It should be noted that even though the 65-μm-core fiber is highly multimode, fundamental mode operation was stable and robust once achieved. The energy of the main pulse was 118 μJ after the 65-μm-core amplifier and 65 μJ after the compressor.

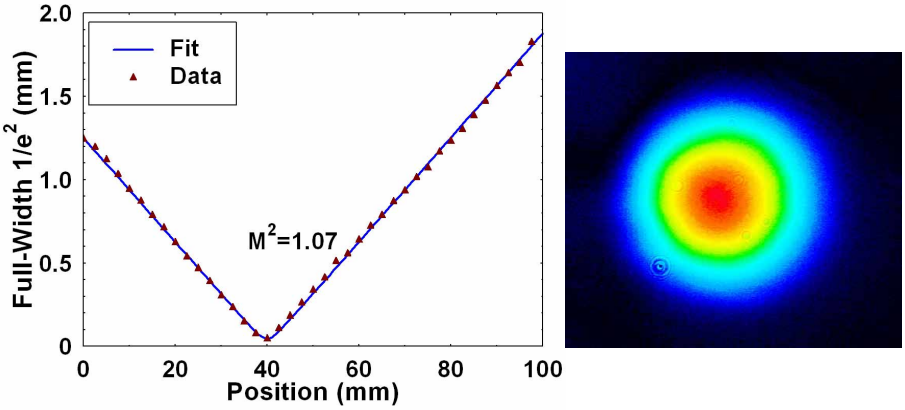

Fig. 2. (a). Beam quality measurement of the 65-μm-core VLMA fiber using knife-edge method with a 75-mm focusing lens. The curve fit of the measured data shows the beam has M^2=1.07. (b). Beam profile measurement with collimated beam using a CCD camera. It shows a symmetrical LP_{01} mode profile with FWHM 2-mm diameter.

A second harmonic frequency-resolved optical gating (FROG) measurement was used to characterize the temporal profile of ~300 fs recompressed pulse. Measured temporal and spectral profiles of the recompressed pulses are shown in Fig. 3. Also, measurements using an InGaAs fast photodiode showed that the contrast ratio is $3x10^{-5}$ to $1x10^{-6}$ between the main pulse and the pre-pulses. The nanosecond-scale pulsed amplified spontaneous emission (ASE) which originated from the inline AOM also showed a contrast ratio of less than $1x10^{-6}$.

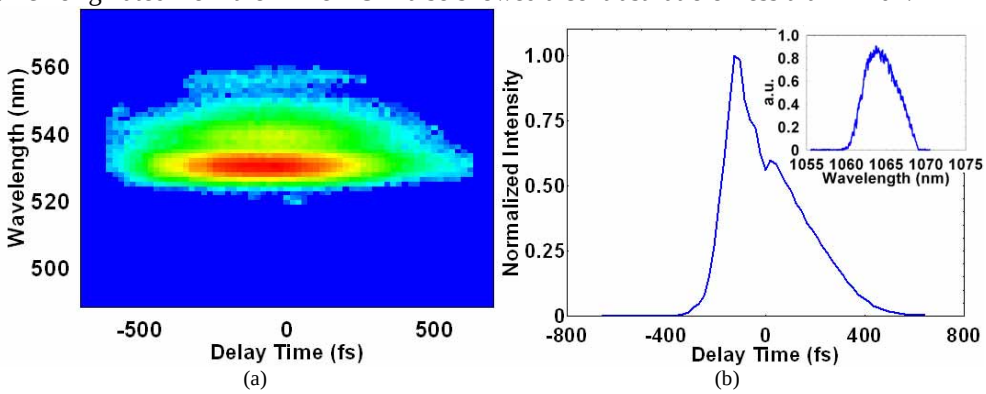

Fig. 3. Frequency resolved optical gating (FROG) measured profile. (a). Original measured profile. (b). Reconstructed temporal profile with 300-fs FWHM and the measured spectrum at 65-μJ recompressed pulse energy.

#86447 - $15.00 USD Received 13 Aug 2007; revised 13 Sep 2007; accepted 22 Sep 2007; published 9 Oct 2007

3. Experiment setup

The X-ray generation set-up is depicted in Fig. 4. For efficient X-ray generation with sub-millijoule pulses it is necessary to achieve on-target focal spot sizes close to the diffraction limit. In the setup, the compressed p-polarized pulses, incident at 45°, are focused on a Ni slab target using an f /1.2, 60° off-axis gold-coated paraboloidal mirror. This focusing optics configuration induced significant beam aberrations, preventing reaching the diffraction-limited focal spot. To compensate for these aberrations a 45-mm diameter deformable mirror (Xinetics Inc) has been used to dynamically optimize beam wavefront. This is achieved by imaging the focal spot onto a second harmonic crystal using a 60× microscope objective to provide feedback in the form of second harmonic light to a genetic algorithm that controls the positions of the mirror's 37 actuators. The combination of small f-number focusing and adaptive wavefront correction ensures a 2.3-μm full width at half maximum (FWHM) focal spot (Fig. 5).

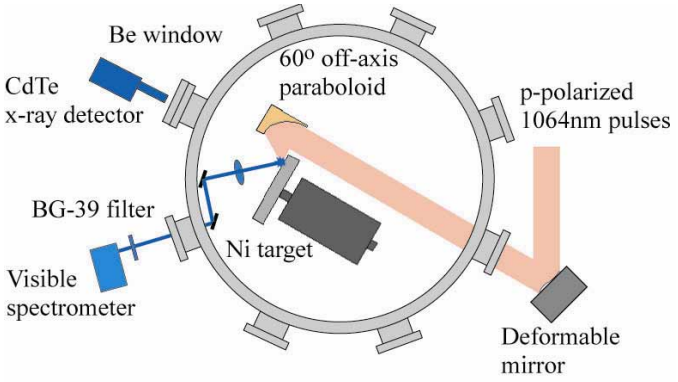

Fig. 4. The fiber laser produced x-ray source experimental chamber. A deformable mirror is used to optimize the focus of an off-axis paraboloidal mirror. The visible spectrometer measures the second harmonic emitted along the specular direction to find the optimum target position. The X-rays are measured with a CdTe cooled detector (Amptek).

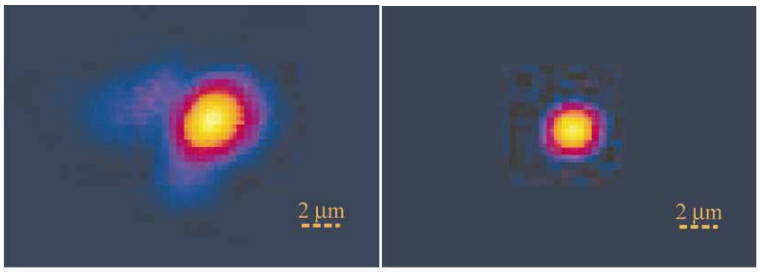

Fig. 5. The laser focal spot imaged by a 60× microscope objective before (a) and after (b) the deformable mirror optimization. The optimized spot full width at half maximum is 2.3μm.

The Ni target is mounted inside the vacuum chamber (10^{-1} mbar) on a motorized stage and rotated to ensure that each laser shot interacts with a fresh area. The micro-plasma is imaged along the specular direction using an f = 100-mm lens onto the entrance slit of a visible spectrometer (Ocean Optics) through a BG39 filter that absorbs the 1064-nm driving light and passes the visible. The target position with respect the focal plane is optimized by maximizing the plasma second harmonic emission. A 2-μm thick pellicle is used to protect the mirror from the debris emitted from the plasma.

The X-ray spectrum is measured using a Cadmium-Telluride diode detector and a multi-channel analyzer from Amptek Inc. (XR-100T-CdTe and MCA-8000A, respectively). The

#86447 - $15.00 USD Received 13 Aug 2007; revised 13 Sep 2007; accepted 22 Sep 2007; published 9 Oct 2007

diode, protected with a 75-μm thick Beryllium (Be) window, has an active area of 9 mm^2, thickness of 1 mm and is thermo-electrically cooled down to -30°C. The detector is mounted along the direction of the target normal 48 cm from the plasma through another 50-μm thick Be window. It was calibrated using an ^{241}Am radioactive source.

4. Result and discussion

At intensities higher than $10^{14}W/cm^2$ a laser pulse can deposit a sizeable fraction of its energy into the plasma electrons through a multitude of processes such as resonant absorption, vacuum and **J**×**B** heating. The resulting hot electrons (with effective temperature *Te*) acquire enough momentum to penetrate deep inside the solid-density target beyond the interaction volume. A fraction of these electrons will scatter off the Coulombic field of the cold nuclei causing them (the electrons) to radiate at photon energies that depends on the impact parameter (field strength). This results in the emission of a broad-band continuum (bremsstrahlung) with a Maxwellian distribution at an effective temperature *Te*. These hot electrons could also knock off an inner-shell (*K*-shell) electron from cold atoms, the subsequent relaxation of which results in narrow line emission ($d\lambda/\lambda \cong 10^{-4}$) at photon energies characteristic of the target material (Z number).

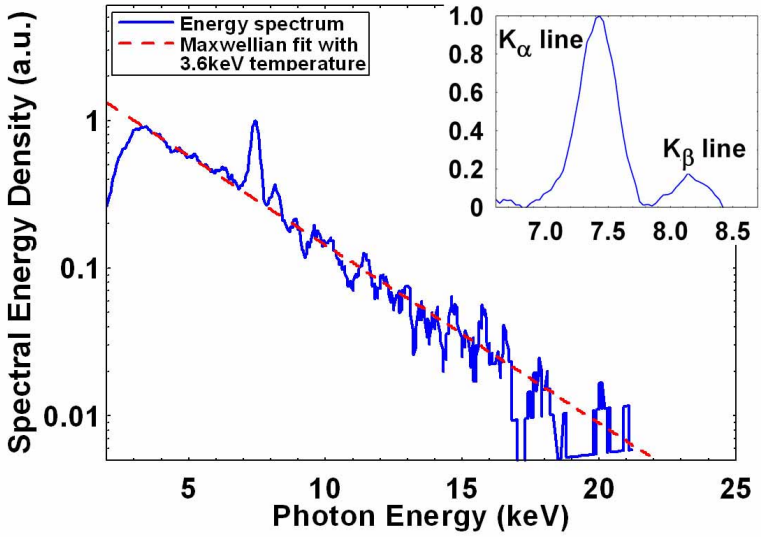

Fig. 6. The Ni plasma spectral energy density per 1-keV bandwidth emitted into the half space per second. The bremsstrahlung extends to photon energies up to 22 keV and corresponds to an electron temperature *Te* = 3.6 keV. The insert shows the bremsstrahlung subtracted relative intensity plot of the K_α and K_β lines on a linear scale. The focal intensity is $I = 2.8\times10^{15}$ W/cm^2 with a pulse energy of 50μJ at the target.

In our experiment the Ni (Z = 28) target was shot at a repetition rate of 1 kHz with 50-μJ pulse energy (on target), corresponding to a focal peak intensity $I = 2.5\times10^{15}$ W/cm^2. The spectrum, shown in Fig. 5, was measured with the CdTe detector operating in single photon count mode (0.15 photon/pulse) for an exposure duration of 80 seconds. The bremsstrahlung extended to energies higher than 20 keV with a single Maxwellian temperature *Te* = 3.6 keV. Its low energy component (0−4keV) is governed by the transmission of the Be filters which become almost fully transparent for photon energies > 4keV. Additionally, the K_α and the K_β lines were observed (Fig. 5 insert) with energy conversion efficiency of 4.5×10^{-8} and 0.6×10^{-8} respectively. The corresponding yield is 2×10^6 K_α photons per second into the half space. The conversion efficiency into the K_α photon is calculated using the following formula:

#86447 - $15.00 USD Received 13 Aug 2007; revised 13 Sep 2007; accepted 22 Sep 2007; published 9 Oct 2007

$$\eta K_\alpha = T_{Be} \cdot \eta_{CdTe} \cdot \frac{2\pi}{\Omega_{CdTe}} \cdot \frac{N_{K_\alpha} \cdot \hbar\omega_{K_\alpha}}{P_{Laser}}$$

Here P_{Laser} is the laser average power on target and N_{K_α} the number of K_α photons – each with an energy of $\hbar\omega_{K_\alpha}$ – detected per second by the CdTe detector. η_{CdTe} is the Ni K_α absorption probability in 1mm-thick CdTe, taken equal to unity since the attenuation length is 4.5μm. T_{Be} is the transmission through both diode (75μm) and vacuum chamber (50μm) Be filters. Ω_{CdTe} is the solid angle subtended by the detector surface seen from the plasma source and is used to estimate the total number of K_α photons emitted in the 2π solid angle assuming an isotropic emission.

This conversion efficiency was comparable with previously published results with similar pulse energy. For a similar pulse energy Hou et al. [6] measured a conversion efficiency of 10^{-7} from a Molybdenum target (Z = 43) using 22 fs laser. In that paper the authors describe a weak dependence of the efficiency on the laser pulse duration $\eta_{K_\alpha} \propto exp(-\tau/\beta)$, where $\beta \cong 650$ fs. This scaling accounts for the factor ~ 2 difference between the work in [7] and this work even though the pulse duration ratio is ~ 15. The dependence on the spot size however seems to be of greater importance. Hagedorn et al. [8] focused 30-fs, 100-mJ pulses to a spot size ~ 10 times larger than the spot size in the present work and yielded an efficiency one order of magnitude less (5×10^{-9}).

5. Conclusion

We have demonstrated the first generation of bremsstrahlung and K_α X-rays from a Ni target using a high energy fiber laser system which provides high temporal repulse contrast ratio ($<2.5\text{x}10^{-5}$) and high quality spatial profile ($M^2 < 1.07$). The X-ray conversion efficiency was comparable with results obtained using shorter but similar-energy pulses from Ti:sapphire systems. An enhancement of ~1−2 orders of magnitude in the K_α efficiency can be expected once the pulse energy on target is increased to the millijoule level. Note that such energies are available from the current FCPA system [6], but requires further increase in the pre-pulse contrast ratio. Furthermore, since fiber lasers are compatible with high average power scaling and higher repetition rate operation (~100 kHz), the brightness of the fiber laser driven K_α source will be adequate for both imaging and time-resolved diffraction experiments. Finally, with the emergence of chirped volume Bragg grating based on photo-thermal-refractive (PTR) glass technology [9], the high energy FCPA system has the potential to be the basis of a compact, monolithic, high-brightness table-top X-ray source.

Acknowledgment

This project is partially supported by the AFOSR MURI grant #FA9550-05-1-0416.

#86447 - $15.00 USD Received 13 Aug 2007; revised 13 Sep 2007; accepted 22 Sep 2007; published 9 Oct 2007